



A preliminary study of super-resolution deep learning reconstruction with cardiac option for evaluation of endovascular-treated intracranial aneurysms

Chuluunbaatar Otgonbaatar , MD^{1,2}, Hyunjung Kim, MD³, Pil-Hyun Jeon, PhD³, Sang-Hyun Jeon, BS³, Sung-Jin Cha, BS³, Jae-Kyun Ryu, PhD², Won Beom Jung, PhD⁴, Hackjoon Shim, PhD^{2,5}, Sung Min Ko, MD, PhD³, Jin Woo Kim , MD^{*,3}

¹Department of Radiology, College of Medicine, Seoul National University, Seoul, 03080, Republic of Korea

²Medical Imaging AI Research Center, Canon Medical Systems Korea, Seoul, 06173, Republic of Korea

³Department of Radiology, Wonju Severance Christian Hospital, Wonju College of Medicine, Yonsei University of Korea, Wonju 26426, Republic of Korea

⁴Korea Brain Research Institute (KBRI), Daegu, 41062, Republic of Korea

⁵ConnectAI Research Center, Yonsei University College of Medicine, Seoul, 03772, Republic of Korea

*Corresponding author: Jin Woo Kim, MD, Department of Radiology, Wonju Severance Christian Hospital, Wonju College of Medicine, Yonsei University of Korea, 20 Ilsan-ro, Wonju, Gangwon 26426, Republic of Korea (sunny-cocktail@hanmail.net)

Abstract

Objectives: To investigate the usefulness of super-resolution deep learning reconstruction (SR-DLR) with cardiac option in the assessment of image quality in patients with stent-assisted coil embolization, coil embolization, and flow-diverting stent placement compared with other image reconstructions.

Methods: This single-centre retrospective study included 50 patients (mean age, 59 years; range, 44–81 years; 13 men) who were treated with stent-assisted coil embolization, coil embolization, and flow-diverting stent placement between January and July 2023. The images were reconstructed using filtered back projection (FBP), hybrid iterative reconstruction (IR), and SR-DLR. The objective image analysis included image noise in the Hounsfield unit (HU), signal-to-noise ratio (SNR), contrast-to-noise ratio (CNR), and full width at half maximum (FWHM). Subjectively, two radiologists evaluated the overall image quality for the visualization of the flow-diverting stent, coil, and stent.

Results: The image noise in HU in SR-DLR was 6.99 ± 1.49 , which was significantly lower than that in images reconstructed with FBP (12.32 ± 3.01) and hybrid IR (8.63 ± 2.12) ($P < .001$). Both the mean SNR and CNR were significantly higher in SR-DLR than in FBP and hybrid IR ($P < .001$ and $P < .001$). The FWHMs for the stent ($P < .004$), flow-diverting stent ($P < .001$), and coil ($P < .001$) were significantly lower in SR-DLR than in FBP and hybrid IR. The subjective visual scores were significantly higher in SR-DLR than in other image reconstructions ($P < .001$).

Conclusions: SR-DLR with cardiac option is useful for follow-up imaging in stent-assisted coil embolization and flow-diverting stent placement in terms of lower image noise, higher SNR and CNR, superior subjective image analysis, and less blooming artifact than other image reconstructions.

Advances in knowledge: SR-DLR with cardiac option allows better visualization of the peripheral and smaller cerebral arteries. SR-DLR with cardiac option can be beneficial for CT imaging of stent-assisted coil embolization and flow-diverting stent.

Keywords: intracranial aneurysm; image reconstruction; super-resolution deep learning reconstruction; blooming artifact; CT angiography.

Introduction

Intracranial aneurysms are weakness in brain vessel wall that bulge outward and can rupture, causing life-threatening consequences. Stent-assisted coil embolization has become a widely accepted safe and effective technique for the endovascular treatment of wide-neck intracranial aneurysm.^{1,2} This technique can reduce the risk of coil protrusion into the parent vessel during the embolization and decrease the recanalization rate.³ Over the past years, flow-diverting stents have been increasingly used for the treatment of giant and wide-neck aneurysms, which aid in intra-aneurysmal stasis by redirecting the circulation in aneurysms.^{4,5}

Computed tomography (CT) angiography is a widely used noninvasive imaging modality that requires a short examination time and is used as pre-procedural imaging for

understanding anatomical variations and treatment planning and as follow-up imaging for identifying residual flow and visualization of kinking, position, and wall apposition of the stent devices after endovascular treatment.⁶ However, CT angiography still faces the challenges of blooming artifact of these metallic devices, which limit its use in the accurate delineation of the vessel lumen and stent due to lower spatial resolution.

Ultrahigh-resolution CT with a small detector cell size (0.25×0.25 mm) and focal spot size (0.4×0.5 mm) was commercially released uniquely by one vendor (Aquilion Precision CT; Canon Medical Systems Corporation, Otawara-si, Japan) and has been reported to offer superior spatial resolution, higher visualization of the small vessel branches, and excellent assessment of follow-up for

post-endovascular treatment.^{7,8} In comparison to more widely used 320-row CT scanner, it has limitations in functions other than spatial resolutions, such as narrower z-axis coverage, longer gantry rotation speed, and, most importantly, lower signal-to-noise ratio (SNR) that is inherent in small detector cell size.⁹⁻¹¹ It would be very beneficial if the image quality, especially the spatial resolution, of 320-row CT images could be improved to the level of ultrahigh resolution CT with a deep learning technology, which outperforms conventional technologies in image quality improvements such as denoising and super-resolution. These benefits can be implemented only by the vendor which commercially released the ultrahigh-resolution CT, which is the only way to obtain the training data of ultrahigh-resolution CT images.

Previous studies have demonstrated that super-resolution deep learning reconstruction (SR-DLR; Precise Image Quality Engine [PIQE] Canon Medical Corporation, Otawara-shi, Japan) offers superior image quality with lower image noise, improved spatial resolution, better delineation of cardiac structures, and higher sharpness than other image reconstruction methods, including conventional deep learning reconstruction (DLR), model-based iterative reconstruction (MBIR), hybrid iterative reconstruction (IR), and filtered back projection (FBP) on coronary CT angiography.^{10,12-14} Currently, PIQE is available for cardiac option,¹⁵ and this limitation ironically motivates the study of using the cardiac option to brain CT angiography of metallic devices, some of which are common to cardiac. We hypothesize that SR-DLR can potentially provide a higher image quality and better visualization of stent-assisted coil embolization and flow-diverting stent compared with other image reconstruction methods. Therefore, this study aimed to investigate the usefulness of SR-DLR with cardiac option for brain CT angiography in assessing image quality in patients who underwent stent-assisted coil embolization, coil embolization, and flow-diverting stent placement compared to those of other image reconstructions.

Methods

This retrospective study was approved by the Institutional Review Board of our hospital, and informed consent was waived. A total of 58 patients (mean age, 59 years; range, 44-81 years; 13 men) who were treated with stent-assisted coil embolization, coil embolization, and flow-diverting stent placement and underwent brain CT angiography after the procedure between January 2023 and July 2023 were included in this retrospective study. The exclusion criteria were severe motion artifact ($n=3$) or incomplete image reconstruction ($n=5$) due to the loss of raw projection data (Figure 1).

CT acquisition

All patients were scanned using a 320-multidetector CT-volume scanner (Aquilion ONE PRISM; Canon Medical Systems Corporation). The scan parameters were as follows: tube voltage, 100 kVp; field of view, 180 mm; detector collimations, 320×0.5 mm; gantry rotation time, 0.275 s; slice thickness, 0.5 mm; and matrix size, 512×512 pixels. Automatic exposure control (^{SURE}Exposure; Canon Medical Systems Corporation) was applied for the tube current. Contrast-enhanced imaging was performed by injecting 60 mL of iodinated contrast medium (Iomeron 400; Bracco

Imaging SpA, Milan, Italy) at a flow rate of 4.5 mL/s and then flushing 30 mL of saline at the same flow rate through a 20-gauge peripheral intravenous catheter. The bolus tracking region of interest (ROI) (^{SURE}Start; Canon Medical Systems Corporation) was placed at aortic bifurcation to check reaching to a threshold of 120 Hounsfield units (HUs). The images were reconstructed using three different methods: FBP, hybrid IR with FC04—standard strength (Adaptive Iterative Dose Reduction 3D; Canon Medical Systems Corporation), and SR-DLR with cardiac standard option (PIQE; Canon Medical Systems Corporation). Postprocessing was performed on Vitrea workstation (Vital Images, MN, United States). The dose-length product (DLP) and CT dose index-volume (CTDI_{vol}) value were collected for each patient.

Objective image analysis

In each patient, a quantitative analysis was performed in 0.5 mm slice thickness of axial source image by a radiologist with five years of experience. The image noise was derived from the standard deviation (SD) of CT attenuation within an ROI composed of two-dimensional spheres with a size of 80 mm² placed in the cerebrospinal fluid of the lateral ventricle. The CT numbers of the cavernous segments of the internal carotid artery (ICA), M1 segment of the middle cerebral artery (MCA), apex of the basilar artery (BA), intracerebral segment of the vertebral artery (VA), and splenius capitis muscle were measured by placing the largest possible ROIs while avoiding the inclusion of vessel wall, calcific plaque, coil, and stent. The SNR was assessed by dividing the CT attenuation of each vessel by its SD. The contrast-to-noise ratio (CNR) was measured as the CT attenuation difference between each vessel and muscle, divided by the noise strength. The image sharpness was evaluated with full width at half maximum (FWHM) using ImageJ software (National Institutes of Health, Bethesda, MD, United States) and OriginPro 2022b (OriginLab Corp., Northampton, MA, United States). The CT attenuation profile was made through the central axis of the intracranial stent, coil, and flow-diverting stent. From the CT attenuation profile, the FWHMs of the stent, coil, and flow-diverting stent were measured.^{14,16,17} The shorter FWHM represented higher sharpness and less blooming artifact.

Subjective image analysis

All images were independently reviewed by two experienced radiologists (with 7 and 20 years of experience in general radiology and neuroradiology). Both radiologists were blinded to the image reconstruction methods and randomly evaluated the image quality with a 5-point Likert scale as follows: the score of 5 (excellent overall image quality, excellent visualization of the stent, flow-diverting, and coil without blurring, excellent visualization of the parent and peripheral vessels, and minimal image noise), the score of 4 (good overall image quality, good visualization of the stent, flow-diverting, and coil with minimal blurring, good visualization of the parent and peripheral vessels, and mild image noise), the score of 3 (moderate overall image quality, acceptable visualization of the stent, flow-diverting, and coil with medium blurring, moderate visualization of the parent and peripheral vessels, and moderate image noise), the score of 2 (poor image quality, poor visualization of the stent, flow-diverting, and coil with substantial blurring, poor visualization of the parent and peripheral vessels, and severe image noise), and the score

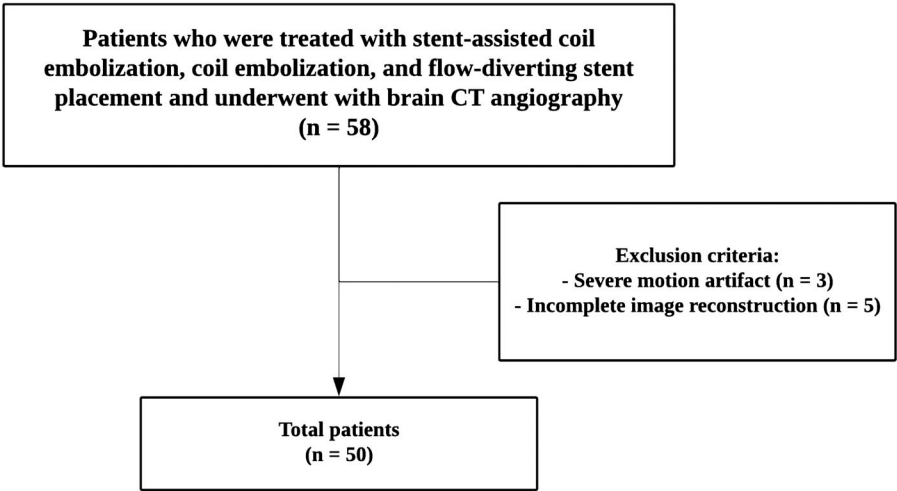


Figure 1. Flowchart of patient enrolment.

of 1 (very poor overall image quality, very poor and not visible visualization of the stent, flow-diverting, and coil, very poor visualization of the parent and peripheral vessels, and very severe image noise).¹⁸

Statistical analysis

Data normality was tested using the Kolmogorov-Smirnov and Shapiro-Wilk tests. Continuous variables were reported as means ± SDs. The CT attenuation, image noise, SNR, CNR, and FWHM were compared among different image reconstructions using one-way analysis of variance, and Tukey *post hoc* test was performed. Qualitative image analysis was performed using the Kruskal-Wallis test among different image reconstructions, and Dunn test was used for multiple comparisons. The interclass correlation coefficient (ICC) with absolute agreement and two-way random effect was used for the observer agreement, where ICC values of <0.5, 0.5-0.75, 0.75-0.90, and >0.9 indicated poor, moderate, good, and excellent agreement, respectively. A *P* < .05 was considered statistically significant. Statistical analysis was performed using SPSS statistical software version 25.0 (IBM, Armonk, NY, United States).

Results

The characteristics of the patients are shown in Table 1. A total of 26 patients were treated with stent-assisted coil embolization, whereas 23 and 3 patients were treated with coil embolization and flow-diverting stent placement, respectively. The aneurysms were located as follows: 12 (23.53%) in the MCA, 11 (21.57%) in the paraclinoid segment of the ICA, 9 (17.65%) in the anterior communicating artery, 8 (15.69%) in the posterior communicating artery, 5 (9.80%) in the BA bifurcation, 4 (7.84%) in the ophthalmic segment of the ICA, 1 (1.96%) in the VA, and 1 (1.96%) in the A2 segment of the anterior cerebral artery. The DLP in mGy · cm was 230.50 ± 30.25 and CTDI_{vol} in mGy was 10.8 ± 1.8.

The results of the CT attenuation, image noise, SNR, and CNR are summarized in Table 2. The mean value of CT attenuation (MCA, ICA, BA, and VA) was not significantly different among the image reconstruction methods, including FBP, hybrid IR, and SR-DLR (*P* = .91). The image noise in HU in SR-DLR was 6.99 ± 1.49, which was significantly

Table 1. Patient characteristics.

Parameters	Total
Age, years	59.24 ± 9.48
Sex, male	13 (26%)
Body mass index, kg/m ²	24.31 ± 3.65
Medical history	
Hypertension	29 (58%)
Diabetic mellitus	8 (16%)
Smoking	8 (16%)
Alcohol	9 (18%)
Hyperlipidaemia	16 (32%)
Location of aneurysm	
ICA, paraclinoid segment	11 (21.57%)
ICA, ophthalmic segment	4 (7.84%)
Posterior communicating artery	8 (15.69%)
Middle cerebral artery bifurcation	12 (23.53%)
Anterior cerebral artery, A2	1 (1.96%)
Anterior communicating artery	9 (17.65%)
Basilar artery bifurcation	5 (9.80%)
Vertebral artery	1 (1.96%)
Endovascular treatment	
Stent-assisted coil embolization	26 (52%)
Neuroform Atlas	23 (46%)
Acandis stent	3 (6%)
Flow-diverting stent placement	3 (6%)
Coil embolization	21 (42%)

Data are reported as mean ± SD. Unless otherwise indicated, data represent the number of patients with percent in parenthesis. Abbreviation: ICA = internal carotid artery.

lower than those for images reconstructed with FBP (12.32 ± 3.01) and hybrid IR (8.63 ± 2.12) (*P* < .001). Tukey *post hoc* test showed a significant difference in all possible pairwise comparisons between different image reconstruction methods (FBP vs hybrid IR, *P* < .001; FBP vs SR-DLR, *P* < .001; hybrid IR vs SR-DLR, *P* < .006). The mean SNR was significantly higher in SR-DLR (53.58 ± 18.97) than in FBP (25.93 ± 8.36) and hybrid IR (34.34 ± 11.39) (*P* < .001). In addition, the CNR was significantly different between FBP (27.93 ± 14.37), hybrid IR (39.37 ± 20.97), and SR-DLR (46.84 ± 24.09) (*P* < .001). Tukey *post hoc* test demonstrated significant differences in both SNR (FBP vs hybrid IR, *P* < .004; FBP vs SR-DLR, *P* < .001; hybrid IR vs SR-DLR, *P* < .001) and CNR (FBP vs hybrid IR, *P* < .001; FBP vs SR-DLR, *P* < .001; hybrid IR vs SR-DLR, *P* < .01) between different

image reconstructions (Figure 2). The results of image sharpness for the stent, flow-diverting stent, and coil are presented in Table 3. The FWHMs for the stent ($P < .004$), flow-diverting stent ($P < .001$), and coil ($P < .001$) were significantly lower in SR-DLR than in FBP and hybrid IR (Figure 3). Tukey *post hoc* test resulted in significant differences between FBP and SR-DLR and hybrid IR and SR-DLR; however, no significant difference was found between FBP and hybrid IR.

Subjective image analysis

The overall image quality of SR-DLR (4.39 ± 0.54) was significantly superior to those obtained by FBP (3.98 ± 0.32) and hybrid IR (3.95 ± 0.29) ($P < .001$). The visualization of the

flow-diverting stent and stent-assisted coil embolization was significantly sharper with less blooming artifact with SR-DLR than with other image reconstructions ($P < .001$). In addition, the visualization of the parent and peripheral vessels was better with SR-DLR because of its higher spatial resolution compared with other image reconstructions, including FBP and hybrid IR (Figure 4). The image noise was scored as mild with SR-DLR (4.44 ± 0.51), while it was scored moderate with FBP (3.95 ± 0.39) and hybrid IR (3.85 ± 0.32) (Table 4). Interobserver agreement was good for overall image quality (ICC, 0.76; 95% confidence interval, 0.66–0.82) and moderate for image sharpness (ICC, 0.61; 95% confidence interval, 0.46–0.71), visualization of the parent and peripheral vessels (ICC, 0.62; 95% confidence interval,

Table 2. The results of computed tomography attenuation, signal-to-noise ratio, contrast-to-noise ratio among different image reconstructions.

	FBP	Hybrid IR	SR-DLR	P value
CT attenuation				
Middle cerebral artery	381.15 \pm 133.65	376.65 \pm 133.41	368.38 \pm 118.64	.87
Internal carotid artery	414.11 \pm 152.91	412.67 \pm 152.78	388.97 \pm 129.86	.60
Basilar artery	351.92 \pm 135.60	347.94 \pm 136.53	352.33 \pm 127.05	.97
Vertebral artery	380.71 \pm 142.01	379.09 \pm 145.47	374.43 \pm 130.03	.98
Mean value	381.97 \pm 137.83	379.09 \pm 138.79	371.03 \pm 124.62	.91
Image noise				
Mean value	12.32 \pm 3.01	8.63 \pm 2.12	6.99 \pm 1.49	.001
Signal-to-noise ratio (SNR)				
Middle cerebral artery	24.85 \pm 10.98	33.21 \pm 14.50	53.16 \pm 25.55	.001
Internal carotid artery	30.23 \pm 13.20	39.40 \pm 17.74	54.40 \pm 25.63	.001
Basilar artery	23.17 \pm 10.00	31.57 \pm 13.68	52.10 \pm 26.71	.001
Vertebral artery	25.47 \pm 9.90	33.19 \pm 13.00	53.87 \pm 22.66	.001
Mean value	25.93 \pm 8.36	34.34 \pm 11.39	53.38 \pm 18.97	.001
Contrast-to-noise ratio (CNR)				
Middle cerebral artery	27.89 \pm 14.00	39.09 \pm 20.27	46.35 \pm 22.96	.001
Internal carotid artery	30.89 \pm 16.45	43.67 \pm 23.60	49.54 \pm 25.14	.001
Basilar artery	25.14 \pm 13.50	35.35 \pm 20.18	44.02 \pm 24.08	.001
Vertebral artery	27.81 \pm 14.58	39.36 \pm 21.52	47.47 \pm 25.08	.001
Mean value	27.93 \pm 14.37	39.37 \pm 20.97	46.84 \pm 24.09	.001

Data are reported as mean \pm SD.

Abbreviations: FBP = filtered back projection; IR = iterative reconstruction; SR-DLR = super-resolution deep learning reconstruction.

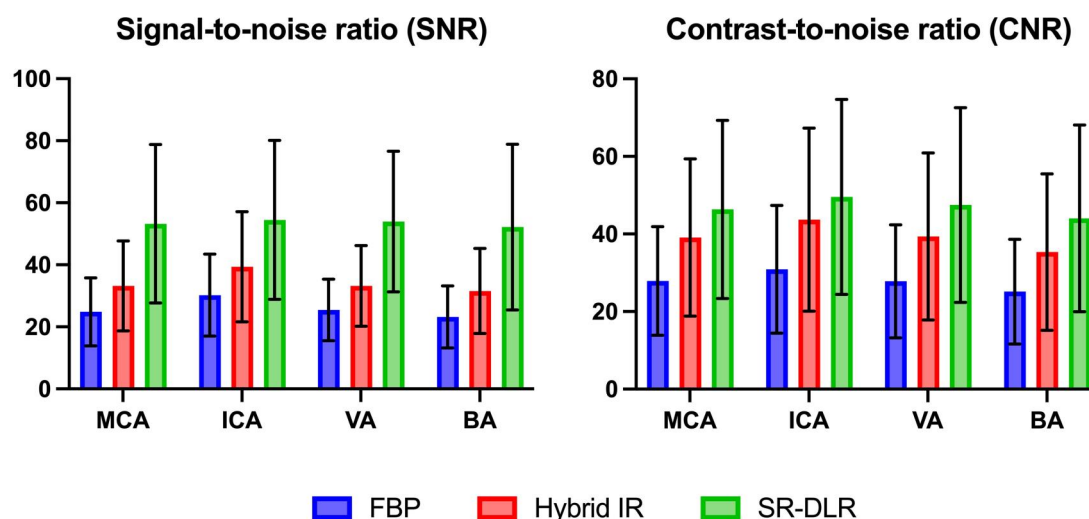


Figure 2. The results of the signal-to-noise ratio (SNR) and contrast-to-noise ratio (CNR) among different image reconstructions. The mean SNR is significantly higher in super-resolution deep learning reconstruction (SR-DLR) (53.58 ± 18.97) than in filtered back projection (FBP) (25.93 ± 8.36) and hybrid iterative reconstruction (IR) (34.34 ± 11.39) ($P < .001$). The CNR is also significantly different between FBP (27.93 ± 14.37), hybrid IR (39.37 ± 20.97), and SR-DLR (46.84 ± 24.09) ($P < .001$). Abbreviations: BA = basilar artery; ICA = internal carotid artery; MCA = middle cerebral artery; VA = vertebral artery.

Table 3. The results of full width at half maximum among different image reconstructions.

	FBP (P_1)	Hybrid IR (P_2)	SR-DLR (P_3)	P value	P_1 versus P_2	P_1 versus P_3	P_2 versus P_3
Full width at half maximum (mm)							
Stent	3.22 ± 1.10	3.18 ± 1.11	2.35 ± 1.03	.004	.74	.01	.01
Flow-diverting stent	4.52 ± 1.04	4.51 ± 1.06	4.19 ± 1.03	.001	.98	.001	.002
Coil	$2.90 \pm .63$	$2.86 \pm .64$	$2.67 \pm .70$.001	.23	.001	.001

Data are reported as mean \pm SD.
Abbreviations: FBP = filtered back projection; IR = iterative reconstruction; SR-DLR = super-resolution deep learning reconstruction.

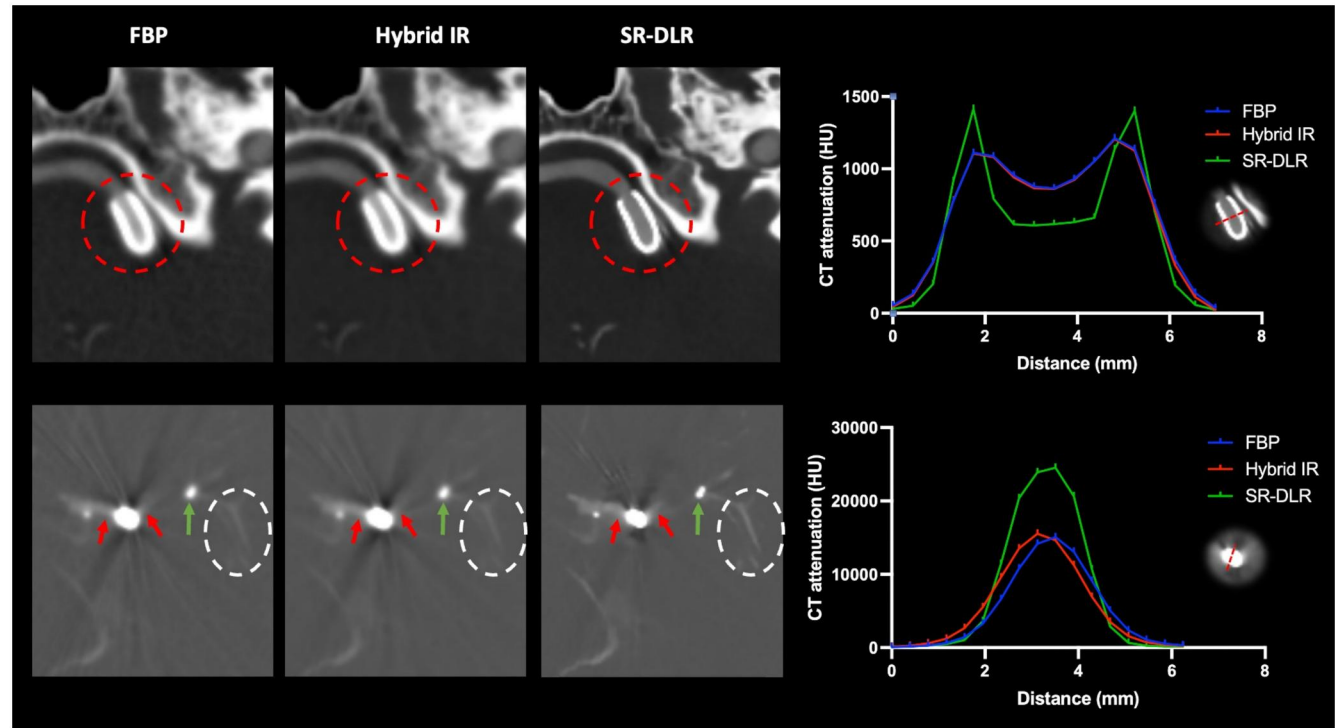


Figure 3. The axial computed tomography angiography from brain for flow-diverting stent placement and stent-assisted coil embolization among different image reconstructions. The visualization of the flow-diverting stent (dashed red circle) and stent-assisted coil embolization (red and green arrows) is sharper with less blooming artifact and well depiction of the intravessel in the flow-diverting stent with super-resolution deep learning reconstruction (SR-DLR) than those with filtered back projection (FBP) and hybrid iterative reconstruction (IR). The higher spatial resolution of SR-DLR results in better visualization of the peripheral arteries than other image reconstructions (white dashed circle). The full widths at half maximum of both the flow-diverting stent and coil are significantly lower in SR-DLR than in other image reconstructions.

0.48-0.72), and image noise (ICC , 0.60; 95% confidence interval, 0.49-0.72). An illustration of the representative cases for flow-diverting stent placement and stent-assisted coil embolization among different image reconstruction is shown in Figure 5.

Discussion

In our study, we observed superior image quality with the use of SR-DLR in patients who underwent endovascular treatment, including stent-assisted coil embolization, coil embolization, and flow-diverting stent placement. The advantages included lower image noise, higher SNR and CNR, superior subjective image analysis, and lower blooming artifact compared to other image reconstructions.

The efficiency for the endovascular procedure and postembolization follow-up imaging is affected by many factors such as full stent deployment, complete wall apposition, full lesion coverage, and its position,¹⁹ and digital subtraction technique using invasive conventional angiography is the gold standard

for evaluation of these factors. However, its invasiveness prevents itself from being follow-up imaging for patients who underwent endovascular treatment, particularly post-flow diverter stent and partially accounts for recanalization, retreatment, and in-stent stenosis of stent-assisted coil embolization, with reported rate of 12%, 6.4%, and 2.5%, respectively.^{20,21} Therefore, for both pre- and post-embolization embolization imaging, there is a critical need for techniques that provide higher spatial resolution and less blooming artifact. Additionally, the interpretation of brain parenchyma adjacent to the coil is also impaired by photon starvation artifact.²²⁻²⁴ Metal artifact reduction algorithms brought significant reduction in artifact adjacent to coil without increasing the radiation dose, but they produce pseudo-stenosis in neighbouring arteries, and their effectiveness varies depending on the size and composition of the metal.^{22,25} Blooming artifacts, caused by the stent, coil, and flow-diverting stent, obscure the vessel lumen. As mentioned earlier, advancement in high-resolution CT hardware and image reconstruction techniques offers promising solutions to address these

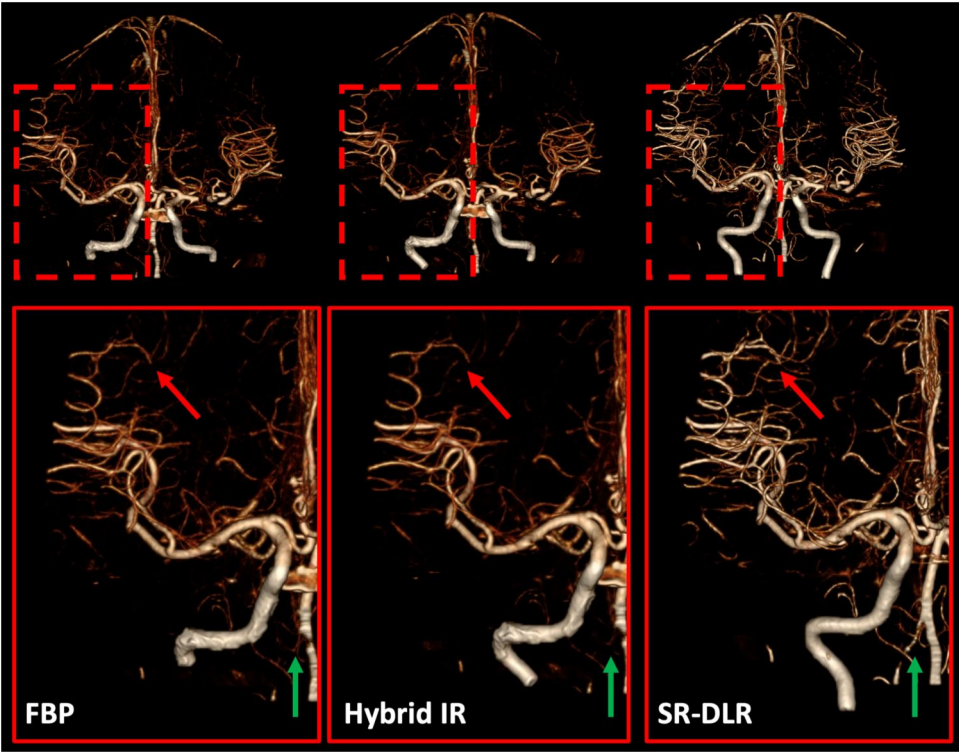


Figure 4. The volume-rendered image of brain computed tomography angiography. Better depiction of the cortical segments of the middle cerebral artery (red arrow) and higher conspicuous visualization of the right vertebral artery (green arrow) is shown in super-resolution deep learning reconstruction (SR-DLR) than filtered back projection (FBP) and hybrid iterative reconstruction (IR). The images are in the same window level and width.

Table 4. The results of subjective image analysis between different image reconstructions.

	Overall image quality	Visualization of the stent, flow-diverting stent, and coil	Visualization of the parent and peripheral vessel	Image noise
FBP	3.98 ± 0.32	4.10 ± 0.33	4.08 ± 0.38	3.95 ± 0.39
Hybrid IR	3.95 ± 0.29	3.93 ± 0.22	3.94 ± 0.24	3.85 ± 0.32
SR-DLR	4.49 ± 0.54	4.54 ± 0.50	4.62 ± 0.51	4.44 ± 0.54
<i>P</i> value	.001	.001	.001	.001
Multiple comparison (<i>P</i> value)				
FBP versus hybrid IR	.99	.06	.18	.70
FBP versus SR-DLR	.001	.001	.001	.001
Hybrid IR versus SR-DLR	.001	.001	.001	.001

Data are reported as mean ± SD.
Abbreviations: FBP = filtered back projection; IR = iterative reconstruction; SR-DLR = super-resolution deep learning reconstruction.

challenges. In hardware factors, utilizing CT hardware with a small detector cell size can improve the spatial resolution and consequently decrease the blooming artifact. Studies by Onishi et al²⁶ and others^{7,27} demonstrate that ultrahigh-resolution CT with a smaller detector cell size significantly enhances the visualization of stents, lenticulostriate arteries, supra-aortic vessel, and small perforating arteries compared to conventional CT. Unfortunately, ultrahigh-resolution CT comes with drawbacks such as higher image noise, narrower z-axis coverage, and lower SNR compared with 320-row normal-resolution CT scanner.^{9-11,28} Photon-counting detector technology, with its ability to measure photon energy in a single semiconductor layer, offers another hardware solution.²⁹ Petritsch et al³⁰ found superior in-stent lumen visibility with photon-counting CT compared with conventional energy-integrating detector CT. Unfortunately, photon-

counting CT is not yet widely available in hospitals. In software factors, deep learning image reconstruction methods have been introduced to improve the image sharpness and decrease the spatial blur.³¹ Several studies have been reported that MBIR improves the image sharpness compared with hybrid IR and normal resolution DLR.^{13,32,33} However, its long reconstruction time limits its widespread use in routine practice.¹⁰ We found the lowest FWHM and highest subjective score of visualization for stent, flow-diverting stent, and coil in SR-DLR than in hybrid IR and FBP. The results of our study are consistent with previous studies investigating image sharpness despite the difference in location and method.^{10,13} SR-DLR allowed for the less blooming artifact of the stents and flow-diverting stents, and better visualization of parent vessels without blurring in CT angiography. Therefore, due to its superior resolution, sharpness, and ability to minimize

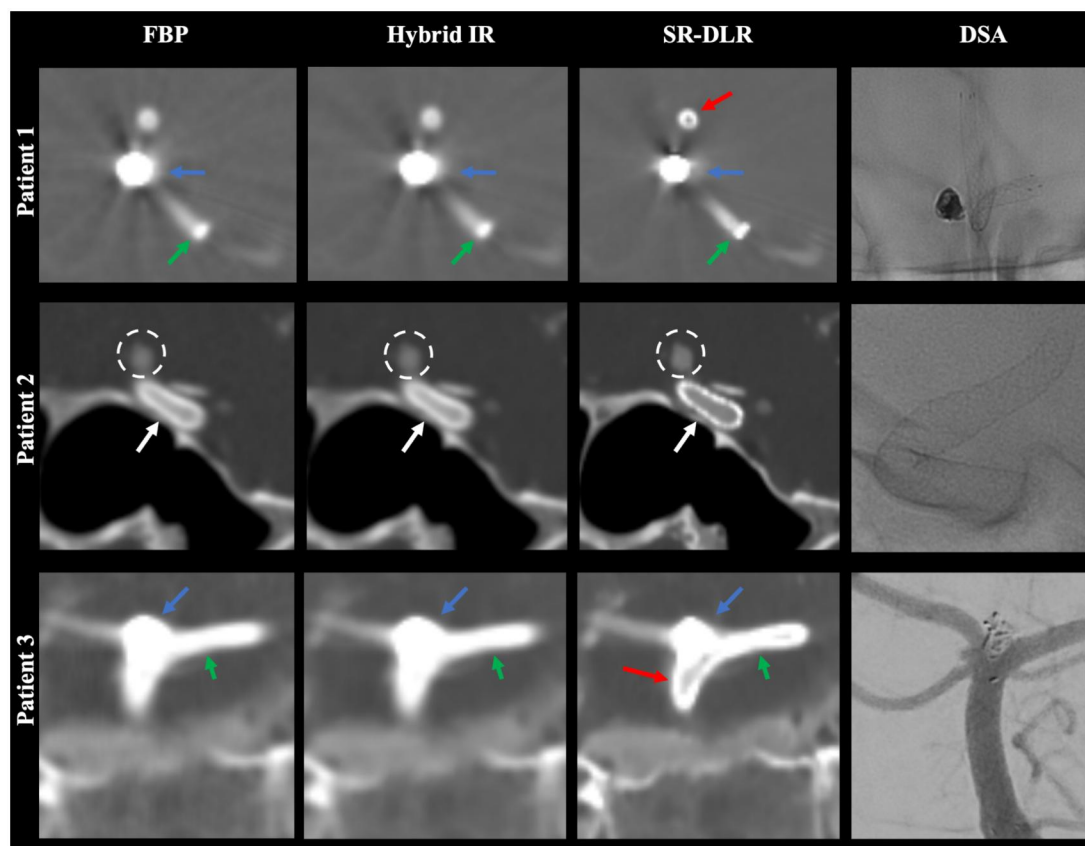


Figure 5. The representative case for flow-diverting stent placement and stent-assisted coil embolization among different image reconstructions. Super-resolution deep learning reconstruction (SR-DLR) shows less blooming artifact in both the stent (green arrow) and coil (blue arrow) than other image reconstructions. The vessel lumen in the stent (red arrow) is clearly demonstrated with less blooming artifact in SR-DLR than those in filtered back projection (FBP) and hybrid iterative reconstruction (IR). The parent vessel (dashed white circle) and mesh structures of the flow-diverting stents (white arrow) are better visualized in SR-DLR than in other image reconstructions. Top row—axial CT angiography; middle row—coronal plane, multiplanar reformation; bottom row—coronal plane, multiplanar reformation. Abbreviation: DSA, digital subtraction angiography.

blooming artifacts, SR-DLR can be beneficial as a tool for follow-up imaging in patients undergoing stent-assisted coil embolization and flow-diverting stent placement.

The results of this study align well with those of the study by Tatsugami et al,¹⁵ who compared the image quality between SR-DLR and hybrid IR in coronary CT angiography. Their study showed that SR-DLR significantly decreased the image noise (51.85%) and improved the CNR (37.03%) compared with hybrid IR. In our study, SR-DLR yielded even better improvement in image noise reduction by 76.25% and 23.46% compared to those in FBP and hybrid IR, respectively, and significantly increased SNR (1.18 and 1.66 times) compared to both FBP and hybrid IR. Additionally, CNR significantly increased in SR-DLR by 1.56 and 2.06 times compared to those in FBP and hybrid IR which was concordant with that of another study.¹³ The image quality and noise in SR-DLR were superior by both observers compared to those in FBP and hybrid IR.

The higher spatial resolution of SR-DLR has the potential to improve visualization of perforators and smaller cerebral arteries, crucial for preoperative treatment planning. Higher image noise and lower resolution in conventional CT angiography reconstructions can sometimes pose challenges in visualizing vessel continuity in small arteries. Therefore, we believe SR-DLR would be desirable to depict the aneurysm shape and full vessel continuity, which would be helpful in

differentiating small aneurysm from a small infundibular dilatation and avoid unnecessary diagnostic subtraction angiography.

This study has several limitations. First, we included a relatively small number of patients in this retrospective study. Second, all patients underwent brain CT angiography directly after postembolization treatment for the follow-up. We have not investigated the diagnostic accuracy for assessing recanalization using different image reconstructions due to lack of reference standard diagnostic subtraction angiography images. Third, all results were limited to one vendor and is limited to cardiac option. However, this is inevitable at this time because only one vendor in the industry is providing SR-DLR, which is available for cardiac CT. Fourth, comparative evaluation did not include normal resolution DLR and MBIR. Future study should investigate the comparison of normal resolution DLR, MBIR, and different SR-DLR options when available, for assessing stent-assisted coil embolization and flow-diverting stent placement, including more patients. While limitation exists, our study demonstrates that SR-DLR with cardiac option significantly improves both objective and subjective image qualities with less blooming artifact than other image reconstructions in brain CT angiography.

In conclusion, SR-DLR with cardiac option is useful for follow-up imaging in stent-assisted coil embolization and

flow-diverting stent placement in terms of higher CNR and SNR, superior subjective image analysis, and lower image noise and blooming artifact than other image reconstructions.

Acknowledgements

We would like to thank Canon Medical Systems Korea, especially Stark Kim and Yoo Donguei (CT application specialist), for assisting with image acquisition.

Author contributions

C. Otgonbaatar and H. Kim contributed equally.

Funding

This research was supported by the KBRI Basic Research Program through the Korea Brain Research Institute and funded by the Ministry of Science and ICT (24-BR-02-02, 24-BR-05-02 to W.B.J.).

Conflicts of interest

The co-authors (C.O., J.K.R., H.S.) are employees of Canon Medical Systems Korea, Seoul, Korea that is the subsidiary in Korea of Canon Medical Systems Corporation, Otawara-si, Japan. Other authors have no relevant financial or non-financial interests to disclose.

References

1. Tähtinen OI, Vanninen RL, Manninen HI, et al. Wide-necked intracranial aneurysms: treatment with stent-assisted coil embolization during acute (<72 hours) subarachnoid hemorrhage—experience in 61 consecutive patients. *Radiology*. 2009;253(1):199-208.
2. Kim J, Han HJ, Lee W, et al. Safety and efficacy of stent-assisted coiling of unruptured intracranial aneurysms using low-profile stents in small parent arteries. *AJNR Am J Neuroradiol*. 2021;42(9):1621-1626.
3. Bechan RS, Sprengers ME, Majoie CB, Peluso JP, Sluzewski M, van Rooij WJ. Stent-assisted coil embolization of intracranial aneurysms: complications in acutely ruptured versus unruptured aneurysms. *AJNR Am J Neuroradiol*. 2016;37(3):502-507.
4. Shehata MA, Ibrahim MK, Ghozy S, et al. Long-term outcomes of flow diversion for unruptured intracranial aneurysms: a systematic review and meta-analysis. *J Neurointerv Surg*. 2022;15(9):898-902.
5. Martínez-Galdámez M, Onal Y, Cohen JE, et al. First multicenter experience using the Silk Vista flow diverter in 60 consecutive intracranial aneurysms: technical aspects. *J Neurointerv Surg*. 2021;13(12):1145-1151.
6. Soize S, Gawlitza M, Raoult H, Pierot L. Imaging follow-up of intracranial aneurysms treated by endovascular means: why, when, and how? *Stroke*. 2016;47(5):1407-1412.
7. Murayama K, Suzuki S, Nagata H, et al. Visualization of lenticulostriate arteries on CT angiography using ultra-high-resolution CT compared with conventional-detector CT. *AJNR Am J Neuroradiol*. 2020;41(2):219-223.
8. Kayano S, Ito A, Endo T, et al. Efficacy of ultra-high-resolution computed tomographic angiography for postoperative evaluation of intracranial aneurysm after clipping surgery: a case report. *Surg Neurol Int*. 2022;13:85.
9. Oostveen LJ, Boedeker KL, Brink M, Prokop M, de Lange F, Sechopoulos I. Physical evaluation of an ultra-high-resolution CT scanner. *Eur Radiol*. 2020;30(5):2552-2560.
10. Nagayama Y, Emoto T, Kato Y, et al. Improving image quality with super-resolution deep-learning-based reconstruction in coronary CT angiography. *Eur Radiol*. 2023;33(12):8488-8500.
11. Takagi H, Tanaka R, Nagata K, et al. Diagnostic performance of coronary CT angiography with ultra-high-resolution CT: comparison with invasive coronary angiography. *Eur J Radiol*. 2018;101:30-37.
12. Greffier J, Pastor M, Si-Mohamed S, et al. Comparison of two deep-learning image reconstruction algorithms on cardiac CT images: a phantom study. *Diagn Interv Imaging*. 2023;105(3):110-117.
13. Nagayama Y, Emoto T, Hayashi H, et al. Coronary stent evaluation by CTA: image quality comparison between super-resolution deep learning reconstruction and other reconstruction algorithms. *AJR Am J Roentgenol*. 2023;221(5):599-610.
14. Takafuji M, Kitagawa K, Mizutani S, et al. Super-resolution deep learning reconstruction for improved image quality of coronary CT angiography. *Radiol Cardiothorac Imaging*. 2023;5(4):e230085.
15. Tatsugami F, Higaki T, Kawashita I, et al. Improvement of spatial resolution on coronary CT angiography by using super-resolution deep learning reconstruction. *Acad Radiol*. 2023;30(11):2497-2504.
16. Fukushima Y, Fushimi Y, Funaki T, et al. Evaluation of moyamoya disease in CT angiography using ultra-high-resolution computed tomography: application of deep learning reconstruction. *Eur J Radiol*. 2022;151:110294.
17. Orii M, Sone M, Osaki T, et al. Super-resolution deep learning reconstruction at coronary computed tomography angiography to evaluate the coronary arteries and in-stent lumen: an initial experience. *BMC Med Imaging*. 2023;23(1):171.
18. Kim YN, Choi JW, Lim YC, Song J, Park JH, Jung WS. Usefulness of silent MRA for evaluation of aneurysm after stent-assisted coil embolization. *Korean J Radiol*. 2022;23(2):246-255.
19. Yang P, Ahmed A, Schafer S, et al. Low-dose volume-of-interest C-arm CT imaging of intracranial stents and flow diverters. *AJNR Am J Neuroradiol*. 2016;37(4):648-654.
20. Chalouhi N, Jabbour P, Singhal S, et al. Stent-assisted coiling of intracranial aneurysms: predictors of complications, recanalization, and outcome in 508 cases. *Stroke*. 2013;44(5):1348-1353.
21. Amenta PS, Dalyai RT, Kung D, et al. Stent-assisted coiling of wide-necked aneurysms in the setting of acute subarachnoid hemorrhage: experience in 65 patients. *Neurosurgery*. 2012;70(6):1415-1429; discussion 1429.
22. Katsura M, Sato J, Akahane M, et al. Single-energy metal artifact reduction technique for reducing metallic coil artifacts on post-interventional cerebral CT and CT angiography. *Neuroradiology*. 2018;60(11):1141-1150.
23. Zopf D, Lennartz S, Pennig L, et al. Virtual monoenergetic images and post-processing algorithms effectively reduce CT artifacts from intracranial aneurysm treatment. *Sci Rep*. 2020;10(1):6629.
24. Hakim A, Pastore-Wapp M, Vulcu S, Dobrocky T, Z'Graggen WJ, Wagner F. Efficiency of iterative metal artifact reduction algorithm (iMAR) applied to brain volume perfusion CT in the follow-up of patients after coiling or clipping of ruptured brain aneurysms. *Sci Rep*. 2019;9(1):19423.
25. Bier G, Bongers MN, Hempel J-M, et al. Follow-up CT and CT angiography after intracranial aneurysm clipping and coiling—improved image quality by iterative metal artifact reduction. *Neuroradiology*. 2017;59(7):649-654.
26. Onishi H, Hori M, Ota T, et al. Phantom study of in-stent restenosis at high-spatial-resolution CT. *Radiology*. 2018;289(1):255-260.

27. Ucar FA, Frenzel M, Abello Mercado MA, et al. Feasibility of ultra-high resolution supra-aortic CT angiography: an assessment of diagnostic image quality and radiation dose. *Tomography*. 2021;7(4):711-720.
28. Shanbhag SM, Chen MY. Ultra-high-resolution coronary CT angiography: the "final frontier"-are we there yet? *Radiol Cardiothorac Imaging*. 2021;3(4):e210196.
29. Rajagopal JR, Farhadi F, Richards T, et al. Evaluation of coronary plaques and stents with conventional and photon-counting CT: benefits of high-resolution photon-counting CT. *Radiol Cardiothorac Imaging*. 2021;3(5):e210102.
30. Petritsch B, Petri N, Weng AM, et al. Photon-counting computed tomography for coronary stent imaging: in vitro evaluation of 28 coronary stents. *Invest Radiol*. 2021;56(10):653-660.
31. Otgonbaatar C, Ryu J-K, Shin J, et al. Improvement in image quality and visibility of coronary arteries, stents, and valve structures on CT angiography by deep learning reconstruction. *Korean J Radiol*. 2022;23(11):1044-1054.
32. Akagi M, Nakamura Y, Higaki T, et al. Deep learning reconstruction improves image quality of abdominal ultra-high-resolution CT. *Eur Radiol*. 2019;29(11):6163-6171.
33. Narita K, Nakamura Y, Higaki T, Akagi M, Honda Y, Awai K. Deep learning reconstruction of drip-infusion cholangiography acquired with ultra-high-resolution computed tomography. *Abdom Radiol (NY)*. 2020;45(9):2698-2704.